Design of the EuCARD high field model dipole magnet FRESCA2

A. Milanese, M. Devaux, M. Durante, P. Manil, J. C. Perez, J. M. Rifflet, G. de Rijk and F. Rondeaux

***Abstract*— This paper reports on the design of FRESCA2, a dipole magnet model wound with Nb_3Sn Rutherford cable. This magnet is one of the deliverables of the High Field Magnets work package of the European FP7-EuCARD project. The nominal magnetic flux density of 13 Tesla in a 100 mm bore will make it suitable for upgrading the FRESCA cable test facility at CERN. The magnetic layout is based on a block coil, with four layers per pole. The mechanical structure is designed to provide adequate pre-stress, through the use of bladders, keys and an aluminum alloy shrinking cylinder.**

***Index Terms* — Dipole magnet, Nb_3Sn, superconducting magnet, EuCARD.**

I. Introduction

THE upgrade of existing accelerator magnets in Europe relies on high current densities and large temperature margins, in order to meet the field and gradient requirements and to withstand the augmented radiation load. Nowadays the appropriate conductor to meet these objectives is Nb_3Sn, because of its superconducting properties and its industrial availability.

Its brittle behavior, strain sensitivity and the increased Lorentz forces in Nb_3Sn magnets demand a careful design, in particular for the mechanical part. As a step towards higher field accelerator magnets, the High Field Magnet task [1] – within the FP7 European project EuCARD – focuses on designing, building and testing a dipole magnet with operational flux density of 13 T in a 100 mm bore. This 1.5 m long dipole will be used to upgrade the FRESCA test facility at CERN, fulfilling the need to qualify conductor at higher fields. The delivery of this magnet (FRESCA2) is scheduled for 2013.

II. Magnetic Design

A. Conductor

The magnetic design is based on a Nb_3Sn strand capable of delivering a critical current density in the superconductor of J_c = 2500 A/mm^2 at 12 T, 4.2 K, and 1250 A/mm^2 at 15 T, 4.2 K [2]. These values are decrease by 10% to take into account cabling degradation. For short sample computations, the critical current density J_c is fitted using Summers law (as written in [3]), with the following parameters: B_{c20} = 28 T, T_{c0} = 18 K, C = 0.90×35000 AT$^{1/2}$mm^{-2}. The same law is used to scale the current from 4.2 K to 1.9 K and to assess the temperature margins.

The copper to non-copper volume ratio is 1.25. The strand diameter is 1 mm, with a target effective filament diameter smaller than 50 micrometers and a Residual Resistivity Ratio (RRR) larger than 200.

The Rutherford cable is rectangular and made up of 40 strands. Cabling tests have been performed, leading to choose a transposition pitch around 120 mm for mechanical stability. The insulation thickness is assumed at the moment equal to 0.2 mm per cable face. Table I summarizes the main parameters for the conductor.

TABLE I. Main Conductor Parameters

Parameter	Unit	
Critical current density J_c,(12 T, 4.2 K)	A/mm^2	2500
Critical current density J_c, (15 T, 4.2 K)	A/mm^2	1250
Assumed cabling degradation	%	10
Copper to non-copper volume ratio	/	1.25
Strand diameter	mm	1
Number of strands	/	40
Cable width (bare)	mm	21.4
Cable thickness at 50 MPa (bare)	mm	1.82
Transposition pitch	mm	120
Insulation thickness (per face)	mm	0.200

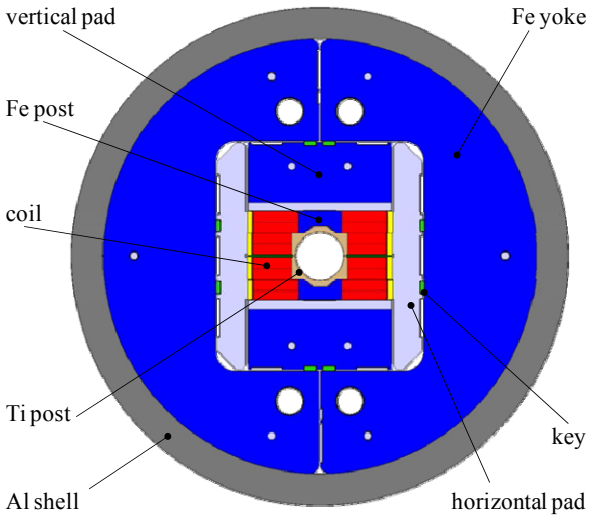

Fig.1. FRESCA2 magnet cross-section.

Manuscript received 7 September 2011. The research leading to these results has received funding from the European Commission under the FP7 Research Infrastructures project EuCARD, grant agreement no. 227579.

A. Milanese, G. de Rijk and J. C. Perez are with CERN, CH-1211 Geneva 23, Switzerland (e-mail: amilanes@cern.ch).

M. Devaux, M. Durante, P. Manil, J. M. Rifflet and F. Rondeaux are with CEA Saclay, 91191 Gif-sur-Yvette, France.

B. Cross-section design

The cross-section of FRESCA2 is shown in Fig. 1. The coil design is based on a block layout [4]. Each pole is made of four layers, wound as two double pancakes. The total number of turns per pole is 156, with 36 spires in layers 1 and 2, and 42 in layers 3 and 4 (the layers are numbered from the midplane outwards). Layers 1 and 2 are formed from a continuous length of cable, and so are layers 3 and 4. The two double pancakes of a pole are individually wound, reacted and instrumented. They are impregnated with the respective central posts and horizontal rails; they are separated by a 1.5 mm thick layer, containing insulation and part of the instrumentation. Between layers 1 and 2 (3 and 4), 0.5 mm are reserved for inter-layer insulation. The 100 mm aperture is given by the assembly of the two inner central posts, without any additional component.

The choice of this 2D layout for the coil, with no spacers in the cross-section and rectangular-like aligned double pancakes, has been favored mostly because it results in a minimum number of discontinuities of geometry and materials around the Nb_3Sn coil. A secondary effect is the expected ease of manufacturing and shimming.

This layout limits *de facto* the number of degrees of freedom available for magnetic optimization to four (not considering the geometry of the iron): the total number of turns, the relative number of spires in coil 1-2 vs. coil 3-4, the position of the first cable in layer 1 and the thickness of the midplane shim. The objectives are multiple: sufficient margin on the load line, field uniformity in the aperture at high current, limited peak field on the coil. The main mechanical constraint is the thickness of the inner central post.

In the baseline coil layout, the first conductor of layers 1 and 2 is wound at a distance of 58 mm from the center, whereas the midplane shim thickness amounts to 2 × 3.5 = 7 mm. These values have been chosen to give a heavier relative weight to field strength with respect to field quality. In this case, in fact, the random harmonics and the nonlinear contribution of the iron (see below) might shadow the importance of reducing the allowable harmonics. Furthermore, the priority for this model is to reach the nominal flux density, with relaxed field quality requirements. Such additional requirements can however be incorporated in the future keeping the same layout.

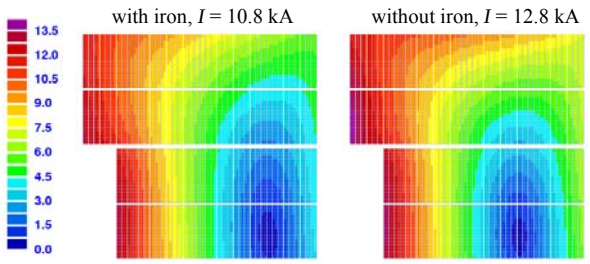

Fig. 2. Magnetic flux density in the coil (T) with and without iron. The flux density in the center is in both cases equal to 13 T. The peak value on the coil in the left figure is 13.2 T, whereas in the right one is 13.9 T.

The following ferromagnetic components are included in the cross-section: the central post for block 3-4, part of the vertical pad and the yoke. These elements have – to a certain extent – different functions. The iron very close to layers 3 and 4 has the effect of reducing the peak field on that region of the coil. The collateral effect is a significant field distortion in the aperture: for example, going for a central flux density B_{center} of 10 T to 13 T, the sextupole b_3 varies by 25.3 units, whereas the decapole b_5 variation is limited to 2.6 units (R_{ref} = 33.33 mm, units in 10^{-4}). If the iron outer post were removed, the b_3 and b_5 changes in the same B_{center} range would be 15.0 and 0.8 units, respectively. The main effect of the iron in the vertical pad and in the yoke, on the other hand, is to increase the field in the aperture for a given current. In fact, the nominal current to attain the design flux density B_{center} = 13 T is 10.8 kA; without iron, this value would rise to 12.8 kA. This has a large impact on the load line but – rather surprisingly – almost none on the lateral Lorentz forces. Secondarily, the stray field is also partially shielded: at nominal field, the maximum stray flux density at 1 m from the center is 100 mT, whereas with no iron it would be 150 mT.

The magnetic flux density in the coil with and without iron is shown in Fig. 2. Although the current is different, the shift in the zero field region in the ironless configuration explains the fact that the lateral Lorentz forces in the two cases are very similar. The main parameters for the magnetic cross section are summarized in Table II; the Lorentz forces at nominal current are listed layer per layer in Table III.

TABLE II. MAIN MAGNETIC CROSS-SECTION PARAMETERS

Parameter	Unit	
Aperture (diameter)	mm	100
Number of turns in layer 1 and 2	/	36
Number of turns in layer 3 and 4	/	42
Inter-layer insulation / inter-blocks insulation	mm	0.5 / 1.5
Midplane thickness	mm	2 × 3.5
Horizont. position of first conductor, layer 1 and 2	mm	58
Radius of iron yoke	mm	450
Nominal magnetic flux density	T	13.0
Nominal current I_{nom}	kA	10.8
Peak flux density on the coil at I_{nom}	T	13.2
Differential inductance per unit length at I_{nom}	mH/m	41.1
Stored energy per unit length at I_{nom}	MJ/m	3.67
Stray magnetic flux density [a] at I_{nom}	mT	100
Central flux density at short sample, 4.2 K / 1.9 K	T	15.5 / 16.7
Short sample current, 4.2 K / 1.9 K	kA	13.2 / 14.4
Load line margin, 4.2 K / 1.9 K	%	18 / 25
Temperature margin at I_{nom}, 4.2 K / 1.9 K	K	3.0 / 5.3
Radius for $\Delta B/B \leq 1\%$ / 2%, at I_{nom}	mm	32 / 42
Sextupole b_3 at nominal current (R_{ref} = 33.33 mm)	10^{-4}	66.8
Decapole b_5 at nominal current (R_{ref} = 33.33 mm)	10^{-4}	−28.1

[a] Taken as the maximum at a distance of 1 m from the center.
The linear dimensions are given at 293 K.

TABLE III. LORENTZ FORCES IN 2D, B_{CENTER} = 13 T

	Horizontal force F_x [MN/m]	Vertical force F_y [MN/m]
Layer 1	1.70	−0.00
Layer 2	1.62	−0.51
Layer 3	2.20	−1.16
Layer 4	2.05	−2.25
Total (one quarter)	7.58	−3.92

The layers are numbered starting from the one closer to the midplane. Negative F_y mean forces towards the midplane.

C. Ends design

The design uses flared coil ends to clear the aperture. This is similar, for example, to HD2 [5] and D10 [6]. From the straight section, the blocks are bent up in the plane of the cable, until an angle of 17 deg is reached; the minimum bending radius is on layer 4 and it is set to 700 mm. A short inclined section follows, with a length of 24 mm for layers 1 and 2, and 31 mm for layers 3 and 4. The ends finally wrap around through circular arcs; the bending radius there is imposed by the cross section layout.

Winding tests with copper cable [7] have guided the choice of the above parameters for the ends geometry. Circular arcs have been preferred over more exotic curves (e.g., clothoids, hyper- and super-ellipses): although the latter have the advantage of theoretically minimizing the local or integrated strain energy of the cable [8], the winding trials suggested that the simplest solution is already satisfactory, given a large enough minimum hard-way bending radius.

The overall coil end-to-end length is set equal to 1500 mm, whereas the minimum straight section is longer than 700 mm. The inclination angle of 17 deg has been chosen after fixing the minimum distance from the midplane to the ends to 61 mm, to accommodate mechanical support. This is a compromise between long planar transitions (large angles) and long inclined sections (small angles), both resulting in shorter straight sections.

The ends also accommodate the layer jumps within the two double pancakes (Fig. 3). Each layer jump comprises two in-plane bends, where the cable bends out towards the central post before connecting to the next turn in the other layer, around a smooth connection curve along the ramp, where the cable is bent in its own plane. The length of the straight section is 730 mm, including the beginning of the jumps. The nominal cable length needed to wind layers 1 is 225 m, whereas 255 m are needed for layers 3 and 4. This results in about 40 km of strand (275 kg) for the overall magnet.

Magnetic simulations in 3D confirm that flux density concentrations in the ends can be controlled by tuning the geometry of the iron and that no spacers are needed in the coil. This seems to be an inherent feature of flared ends, whereas for flat racetrack coils field concentrations are present in the ends if no spacers are added [9], [10]. The geometry of the iron, considering also manufacturing aspects, has been chosen as follows (Fig. 4): the iron yoke covers all the axial length of the magnet, whereas the iron in the vertical pad is extruded above the straight section part only. Finally, the central post of layers 3 and 4 is a solid piece of iron. With this configuration the peak flux density in the coil ends is reduced by 1.0 T with respect to the straight section, at nominal current.

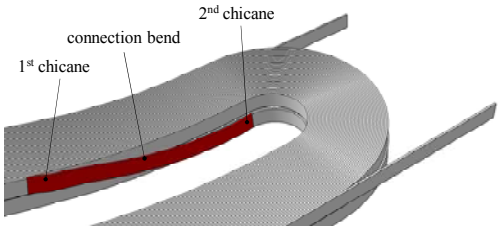

Fig. 3. Layer jump between layers 3 and 4.

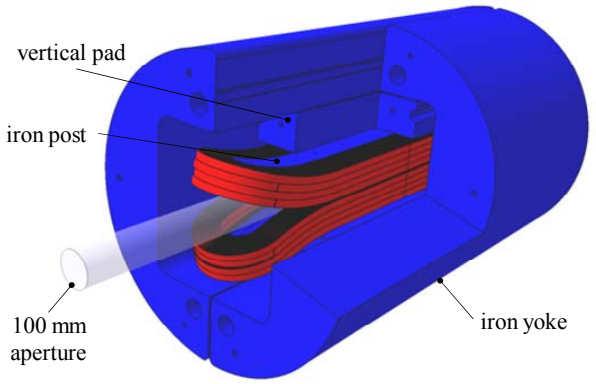

Fig. 4. 3D iron configuration around the coils (cutaway view).

The magnetic length and total stored energy at nominal current are 1.23 m and 3.6 MJ, respectively. The 3D Lorentz forces at nominal current (per octant) are $F_x = 5.06$ MN, $F_y = -2.11$ MN and $F_z = 0.70$ MN, in the horizontal, vertical and axial direction, respectively.

III. Mechanical Design

The mechanical structure is based on the so-called bladder and key concept. This approach was developed at LBNL [11] and it has been successfully used in several model magnets.

With reference to Fig. 1, the coil is surrounded by pads in the horizontal and vertical directions. These pads transfer forces to the outside split iron yoke through keys (mostly in the perpendicular directions). These forces on the iron are finally contained by a 65 mm thick aluminum alloy cylinder. During assembly, bladders are inserted next to the keys and pressurized, in order to create a clearance. This is used to shim the keys before the bladders are removed, so that the final assembly at room temperature involves interferences. The coil is equally compressed on average both on the central post side and on the pad side. During cool-down, the external cylinder tends to shrink more than the other components and provides an additional pre-stress to the coil. During powering, the Lorentz forces tend to separate the coils from the central islands, so that these interfaces are gradually unloaded as the current in the magnet rises.

The design aims at providing adequate pre-stress to the coil throughout the various stages, in particular limiting peak stresses at cryogenic temperatures and maintaining the cable supported along the central posts at the nominal current. The general strategy here is to provide full pre-stress with respect to the Lorentz forces.

The two double layers experience different Lorentz forces (F_x for block 3-4 is about 30% more than for block 1-2). Furthermore, they see a different stiffness in the central region, as in the case of block 1-2 a rather thin titanium alloy island is used, whereas for block 3-4 a solid iron piece is present. Titanium alloy has been chosen because of its high stress carrying capability and for its thermal contraction behavior; the choice of the iron post comes mostly from magnetic considerations. Two lateral keys per side are used instead of a single one: in this way, the forces are better aligned with the coil, especially around the ends. The horizontal pad is in stainless steel; the vertical pad is made of

a stainless plate in contact with the coil and has an iron insert along the straight section. The midplane shim is in G11.

The nominal horizontal interference for a proper lateral preload around the coil at 13 T is 0.60 mm. These computations are based on an assumed friction coefficient between the shell and the yoke equal to 0.2. Simulations show that such an interference can be locked in using reasonable pressures in the bladders (in the order of 300 bar). The average pressures between coil and central post, and between coil and horizontal pads, are reported in Table IV for three steps: room temperature after key insertion, cryogenic temperature, and for a central flux density of 13 T. The pressure at 293 K and 4.2 K is more uniform on the coil-to-rail interface, whereas on the coil-to-central-post side it decreases from the midplane outwards (i.e., from layer 1 to layer 4). This effect is in part unavoidable, due to the presence of the bore, and in part wanted, to better match the distribution of the Lorentz forces. The expected horizontal stresses developed in the coil at 4.2 K and at nominal current are shown in Fig. 5. After cool-down, the maximum horizontal stress in the coil is 135 MPa. At 13 T a peak of 150 MPa is observed, but the high stress and high field region do not overlap. For the impregnated coil, an isotropic Young modulus of 30 / 42 GPa is used at 293 / 4.2 K, with an integrated thermal contraction of 3.36 mm/m.

TABLE IV. AVERAGE LATERAL PRESSURES (MPA) AROUND THE COIL

	coil / central post			coil / lateral rail		
	293 K	**4.2 K**	**13 T**	**293 K**	**4.2 K**	**13 T**
Layer 1	15	35	35	30	60	85
Layer 2	35	90	35	40	80	105
Layer 3	55	120	10	50	100	115
Layer 4	60	130	5	55	120	125

As the structure will be instrumented with strain gauges, the interference values can be adjusted during assembly and after thermal cycles to tune the pre-stress of the coil. To get enough margin of maneuver, about half the pre-stress is given during assembly, and the other half is gained during cool-down. The maximum von Mises stress in the outer shell is 200 MPa.

Looking at the 3D structure (see Fig. 6), the flared coils are supported by two steel wedges on the midplane, while the vertical pads follow the flared shape, getting progressively thinner. The coil blocks are completed with lateral rails and stainless endshoe pieces (reacted and impregnated with the conductor), to reach an axial length of 1.6 m, i.e. the length of the shell.

A longitudinal pre-compression system, similar for example to the one of HD2 [5] and SMC [12], is present: four aluminum alloy rods are pre-tensioned and convey their load to the wedges / endshoes by means of a high resistance steel end plate. This last component is heavily loaded in bending; moreover, its design has to take into consideration the space needed for keys, bladders, as well as instrumentation wires out of the coil. Its thickness has been fixed to 150 mm on the basis of 3D finite element simulations.

The mass of the magnet is around 10 t; the yoke contributes with more than 5 t. The overall diameter is 1030 mm.

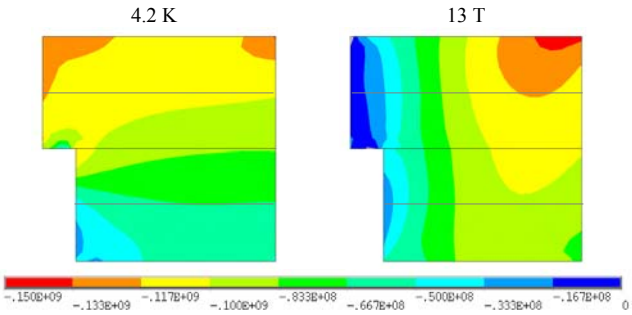

Fig. 5. Horizontal stress in the coil (Pa) after cool-down (left) and at 13 T (right).

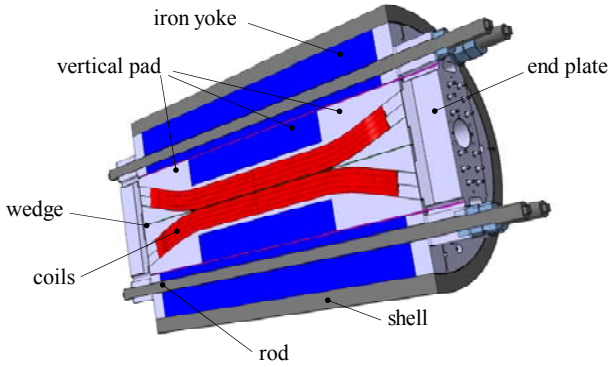

Fig. 6. FRESCA2 magnet structure (longitudinal cutout).

ACKNOWLEDGMENT

We thank all the colleagues with whom we discussed the design of FRESCA2, in particular G. Ambrosio, M. Bajko, B. Bordini, L. Bottura, S. Caspi, P. Fabbricatore, P. Ferracin, G. Kirby, F. Kircher, Y. Iwasa, P. Labrune, J.-F. Millot, T. Nakamoto, L. Oberli, A. Przybylski, L. Rossi and E. Todesco.

REFERENCES

[1] G. de Rijk, "The EuCARD High Field Magnet project," these Proceedings, and "The EuCARD Project," http://eucard.web.cern.ch.

[2] B. Bordini *et al.*, "Extensive characterization of the 1 mm PIT Nb_3Sn strand for the 13-T FRESCA2 magnet," these Proceedings.

[3] A. Devred, "Practical low-temperature superconductors for electromagnets," CERN Report CERN-2004-006, p. 44.

[4] M. Devaux-Bruchon *et al.*, "EuCARD-HFM dipole model design options," EuCARD-REP-2010-002, Oct. 2010.

[5] P. Ferracin *et al.*, "Recent test results of the high field Nb_3Sn dipole magnet HD2," *IEEE Trans. Appl. Supercond.*, vol. 20, no. 3, Jun. 2010, pp. 292-295.

[6] C. Taylor *et al.*, "A Nb_3Sn dipole magnet reacted after winding," *IEEE Trans. Magn.*, vol. MAG-21, no. 2, Mar. 1985, pp. 967-970.

[7] F. Rondeaux, A. Przybylski, P. Manil, "Rapport sur les essais de cintrage des têtes de bobine," CEA note n°SAFIRS-00152-A, May 2010.

[8] A. Milanese, "Shapes of coil ends in racetrack layout for superconducting magnets," CERN TE-Note-2010-04, 2010.

[9] H. Felice *et al.*, "Design and test of a Nb_3Sn subscale dipole magnet for training studies," *IEEE Trans. Appl. Supercond.*, vol. 17, no. 2, Jun. 2007, pp. 1144-1148.

[10] P. Manil *et al.*, "Magnetic design and code benchmarking of the SMC (Short Model Coil) dipole magnet," *IEEE Trans. Appl. Supercond.*, vol. 20, no. 3, Jun. 2010, pp. 184-187.

[11] S. Caspi *et al.*, "The use of pressurized bladders for stress control of superconducting magnets," *IEEE Trans. Appl. Supercond.*, vol. 11, no. 1, Mar. 2001, pp. 2272-2275.

[12] F. Regis, P. Manil, P. Fessia, M. Bajko, and G. de Rijk, "Mechanical design of the SMC (Short Model Coil) dipole magnet," *IEEE Trans. Appl. Supercond.*, vol. 20, no. 3, Jun. 2010, pp. 204-207.